ELSEVIER

Journal of Alloys and Compounds 300–301 (2000) 158–164

Journal of ALLOYS AND COMPOUNDS

www.elsevier.com/locate/jallcom

Photoacoustic spectroscopy of YAG crystals doped with Ce

Marek Grinberg[a,*], Anna Sikorska[a], Slawomir Kaczmarek[b]

[a]*Institute of Experimental Physics, Gdańsk University, Wita Swosza 57, 80-952 Gdańsk, Poland*
[b]*Institute of Optoelectronics, Military University of Technology, Kaliski 2 00-908 Warsaw, Poland*

Abstract

The absorption, luminescence and photoacoustic spectra of YAG:Ce^{3+} have been measured and analysed. Considering the photoacoustic and absorption spectra one has shown a decrease of the quantum efficiency of the Ce^{3+} below 90% when luminescence is excited in the UV region. Simulation of the kinetics of nonradiative processes in the excited states of Ce^{3+} and hot luminescence has been performed. The Jahn–Teller type coupling in the excited states of Ce^{3+} has been evidenced.

Keywords: Insulators; Electron–phonon interaction; Optical properties; Luminescence, Photoacoustic effect

1. Introduction

Electronic structure and optical properties of the Ce^{3+} ions in $Y_3Al_5O_{12}$ (YAG) crystal are determined by the 4f- and 5d-electronic levels split by the spin-orbit interaction and the crystal field of D_2 symmetry. One observes the broad double band green–yellow luminescence and five broad absorption bands, related to 4f–5d transitions. The purpose of this paper is to analyse the nonradiative processes in the excited states of the Ce^{3+} ion and quantum efficiency of the system. We have at our disposal YAG monocrystals doped with Ce of a concentration between 0.05 and 0.2%. The details concerning the material preparations are described elsewhere [1,2]. In this paper we present the optical and photoacoustic (PA) spectra of YAG with high concentration of Ce (0.2%). We have analysed the standard spectroscopy (emission absorption spectra), and photoacoustic spectra of the material. The interpretation of standard spectroscopy experiments allowed us to calculate the parameters of the configurational coordinate diagram describing the energetic structure of the system. Then we modelled the nonradiative processes in the excited states of Ce^{3+}. Our calculation yields the conclusion that the homogeneous broadening of the absorption bands are related to the coupling of the system in the d_1 and d_2 states to the local lattice vibrations of various symmetry.

2. Experimental method

The PA signal results from generation of alternate heat flux in a sample, which is optically excited by a chopped beam of light. The periodical heat flux causes periodical changes of the sample surface temperature and in consequence the overpressure in gas filling the photoacoustic chamber. The investigated samples were $l_s = 1$ mm thick plates so they could be regarded as thermally thick ($l_s \gg \mu$, where thermal diffusion length is given by the expression: $\mu = 1/a_s$ where a_s is a thermal diffusivity of the sample and ω_l is a frequency of excitation modulation). For this case, according to the Rosencwaig–Gersho theory [3], improved by MacDonald et al. [4], following expression for pressure changes in the photoacoustic cell can be derived:

$$P = -\frac{i\gamma \cdot I_0 P_0}{2\omega_l \cdot l_g \rho C_p}\left(\frac{\beta}{\sigma T_0(g+1)(r+1)} + \beta_T[1-\exp(-\beta \cdot l_s)]\right). \quad (1)$$

Here P is the complex signal amplitude, I_0 is the incident light intensity, P_0 and T_0 are the ambient pressure and temperature, respectively, $\gamma = C_p/C_v$ is the ratio of the

*Corresponding author.

0925-8388/00/$ – see front matter
PII: S0925-8388(99)00716-1

specific heats of the samples, l_g is the thickness of the gas layer in the photoacoustic cell, β, ρ and β_T are absorption, density thermal and expansion coefficient of the sample, respectively; g, r and σ are the complex parameters:

$$g = \frac{k_g \cdot a_g}{k_s \cdot a_s}, r = (1-i)\frac{\beta}{2a_s}, \sigma = (1+i)a_s \quad (2)$$

where k_g, k_s and a_g, a_s denote the thermal conductivity and thermal diffusivity for gas and the sample, respectively.

In the original models [3,4] it is assumed that one deals only with instantaneous and pure nonradiative transitions. In order to account for the existence of radiative transitions, the expression (1) should be modified by the factor $\eta = Q/\hbar\Omega$ where Q is the amount of the heat generated in the sample excited by a photon of energy $\hbar\Omega$. Usually the thermal expansion coefficient and sample thickness is small enough to neglect the second term in the parentheses of Eq. (1). In such a way the measured photoacoustic amplitude may be described by the following simplified relation:

$$P = A \cdot I_0(\hbar\Omega) \cdot \eta(\hbar\Omega) \cdot \beta(\hbar\Omega). \quad (3)$$

Here the coefficient A is an apparatus factor independent of the excitation energy. In order to account for spectral characteristics of a light source, $I_0(\hbar\Omega)$, the sample spectrum is calibrated with a blackbody reference spectrum. Thus the quantity that is considered as PA signal from the sample is

$$P_{pas} = A \cdot \eta(\hbar\Omega) \cdot \beta(\hbar\Omega). \quad (4)$$

The PA spectra were carried out with 1 nm step in the wavelength range 270 to 550 nm using an SPM2 monochromator. The photoacoustic cell used was of a transmission type and was equipped with a 1/2-inch condenser microphone SV02 assembled to the SV01 preamplifier (Svantek, Poland). The Stanford Research, dual phase SR 850 lock-in amplifier driven by a computer was used for the signal registration and data acquisition. The modulation frequency 42 Hz was chosen for registration of the PA spectra. All PA spectra were calibrated with a carbon black reference. The measurements were taken at room temperature. Experimentally determined thermal diffusivity of YAG monocrystals is about 3.6×10^{-2} cm^2/s [5]. For the modulation frequency used, $\omega = 42$ Hz, this corresponds to the depth of sample penetration $\mu \approx 1.6\times10^{-2}$ cm. As for the whole range of photon energies the sample absorption coefficient β does not exceed the value of 30 cm^{-1}, the condition for photoacoustic signal nonsaturation: $\beta\mu < 1$ was fulfilled in this spectral range. Luminescence was excited by a xenon lamp and detected with an SPM2 monochromator and photomultiplier. Absorption was measured by a standard Specord photometer. All equipment was controlled by a computer.

3. Configuration coordinate diagram of the Ce^{3+}

To obtain the configuration coordinate diagram of the Ce^{3+} system besides the photoacoustic spectra, the absorption and emission spectra have been measured. All spectra are presented in Fig. 1. The double band seen in the emission spectra is related to $^2F_{5/2}$–$^2F_{7/2}$ ground state splitting. One can see that the photoacoustic spectrum reveals evident structure related to the f→d internal transition in the Ce^{3+} ion, indicated as d_1 d_2 d_3 and d_4. Whereas the d_1 and d_2 bands are very similar in the absorption and photoacoustic spectra the d_3 and d_4 bands are much better seen by the photoacoustic method. We have related this effect to decrease of the quantum efficiency of the Ce^{3+} system when it is excited to the d_3 and d_4 states. For analysis of the energetic structure of the Ce^{3+} ion we have considered also the hot luminescence related to $d_2 \rightarrow {}^2F_{5/2}$–$^2F_{7/2}$ transitions, measured by Suzuki et al. [6]. Since we have not measured the hot luminescence ourselves we have not indicated them in Fig. 1. The structure seen in the absorption at the region of 40,000–50,000 cm^{-1} is probably related to creation bound excitons.

Considering the positions of the bands and their half-widths we were able to reproduce the configuration coordinate diagram of the Ce^{3+} ion (Fig. 2). This diagram has been obtained assuming that the system is coupled to the lattice only by the interaction with one-dimensional, symmetrical local vibration mode. The spectroscopic data yield the information about the absolute value shifts of the particular excited electronic manifold in the configuration space with respect to the ground electronic manifold, whereas the predictions concerning the relative shifts between the excited states are still ambiguous. Let us focus on the d_1 and d_2 electronic manifolds. Considering the absorption bands, luminescence, (Fig. 1), and the hot luminescence [6] one obtains the electron–lattice coupling

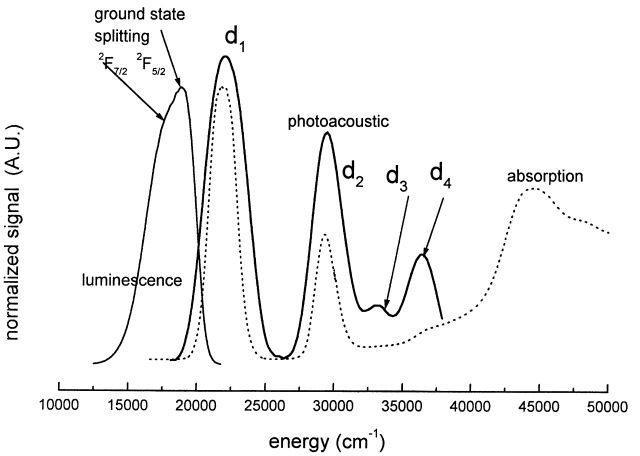

Fig. 1. Luminescence, absorption and photoacoustic spectra of YAG:Ce^{3+}.

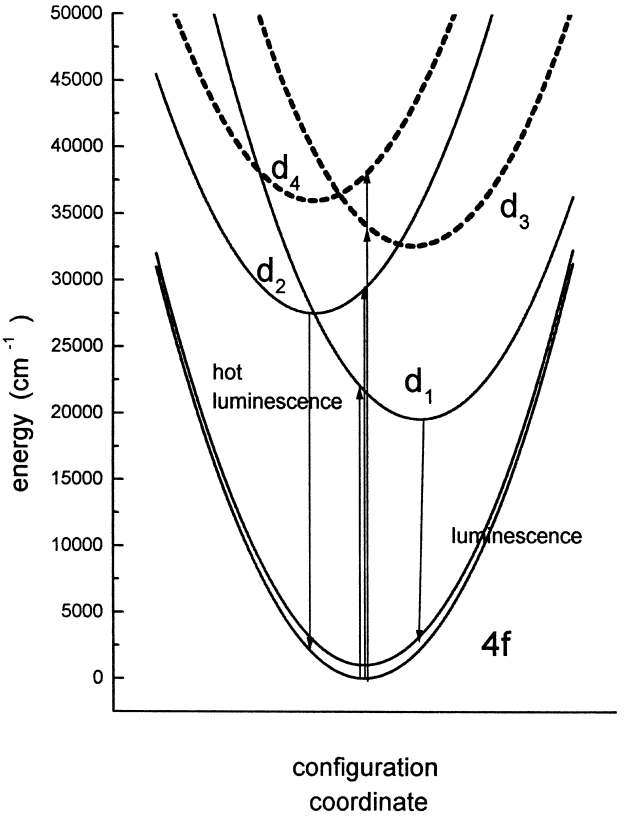

Fig. 2. Single-dimensional configuration coordinate diagram of the YAG:Ce^{3+} system. The diagram has been derived from the spectroscopic data presented in Fig. 1.

energies of the d_1 and d_2 states with respect to the ground state equal to $S_1\hbar\omega = 2225$ cm^{-1} and $S_2\hbar\omega = 1785$ cm^{-1}, respectively. The ambiguity relies on the fact that in the frame of one dimensional configurational space one obtains two equivalent d_1–d_2 relative electron–lattice coupling energies $S_{12}\hbar\omega = 7996$ cm^{-1} and $S_{12}\hbar\omega = 25$ cm^{-1}, depending on whether the manifolds are shifted in the same or in the opposite directions. Since the latter case practically excludes the nonradiative internal conversion between d_2 and d_1 electronic manifolds we present only the former one in the diagram in Fig. 2. One can see that all these relations concern the lattice relaxation energy and do not depend separately on the Huang–Rhys parameter and local phonon mode energy. Actually since we have not seen the phonon structure in the absorption and emission bands we cannot estimate the phonon energy with good accuracy. The only possibility is to analyse the second and third moment of the spectrum. Considering these moments for the absorption one can obtain the phonon energy of the order of 200 cm^{-1}. In the configuration coordinate diagram we have not indicated the dimension of the ion displacements. Usually the dimension of the configuration coordinate is $\sqrt{\hbar/\mu\omega}$, where μ is effective mass of the system and ω is the frequency of local mode. Since we do not know the effective mass as well as the phonon energy we do not put the quantitative units in Fig. 1.

4. The nonradiative processes

Considering the photoacoustic and absorption spectra one can get the information about relative quantum efficiency of the system. Specifically the quantity that can be calculated is relative efficiency of the nonradiative processes (the heat emitted per single absorbed photon):

$$\eta(\hbar\Omega) \propto \frac{P_{\mathrm{pas}}(\hbar\Omega)}{\beta(\hbar\Omega)}. \tag{5}$$

Here P_{pas} is given by (4). Unfortunately we have not measured the photoacoustic and absorption spectra using the same spectrometer. This is a reason why, to avoid the errors related to apparatus spectral resolution, we have considered the integrated absorption and photoacoustic signal. Thus we have estimated relative efficiency of the nonradiative process under particular excitation $\hbar\Omega_{\mathrm{k}}$ using the relation:

$$\eta(\hbar\Omega_{\mathrm{k}}) \propto \frac{\int_{\Omega_{\mathrm{k}}-\Omega_0}^{\Omega_{\mathrm{k}}+\Omega_0} \mathrm{d}\Omega P_{\mathrm{pas}}(\hbar\Omega)}{\int_{\Omega_{\mathrm{k}}-\Omega_0}^{\Omega_{\mathrm{k}}+\Omega_0} \mathrm{d}\Omega \beta(\hbar\Omega)}. \tag{6}$$

Here $2\Omega_0$ is the integration range, which should extend over the whole single band. In such a way one obtains the 'experimental efficiency' for several excitation energies. We have performed calculations dividing all spectra into three parts. The first corresponds to the d_1 band, the second corresponds to the d_2 band and the third corresponds to the d_3 and d_4 bands. The results are presented in Fig. 3. It is seen that the heat emitted per one absorbed photon increases with the excitation energy. One can assume that only nonradiative processes take place during the thermalization of the system in the excited electronic manifold. Under this approximation one obtains the dependence of quantum efficiency on excitation energy given by:

$$\eta(\hbar\Omega) = \frac{\hbar\Omega - \hbar\Omega_{\mathrm{lum}}}{\hbar\Omega} \tag{7}$$

where $\hbar\Omega_{\mathrm{lum}}$ is the energy of the maximum luminescence band. We have taken $\hbar\Omega_{\mathrm{lum}} = 17{,}314$ cm^{-1} from the first moment of the emission lineshape. If the formula (7) is valid it means that after excitation the system relaxes nonradiatively to the d_1 state from which only the radiative deexcitation is possible. Thus, although the system emits heat its quantum efficiency is still equal to unity. The dashed line in Fig. 3 corresponds to the theoretical nonradiative transition efficiency calculated according to (7). It is easy to see that experimental η increases with energy much faster than it is predicted by formula (7). This is a reason one has to consider also the internal conversion nonradiative transitions between the excited

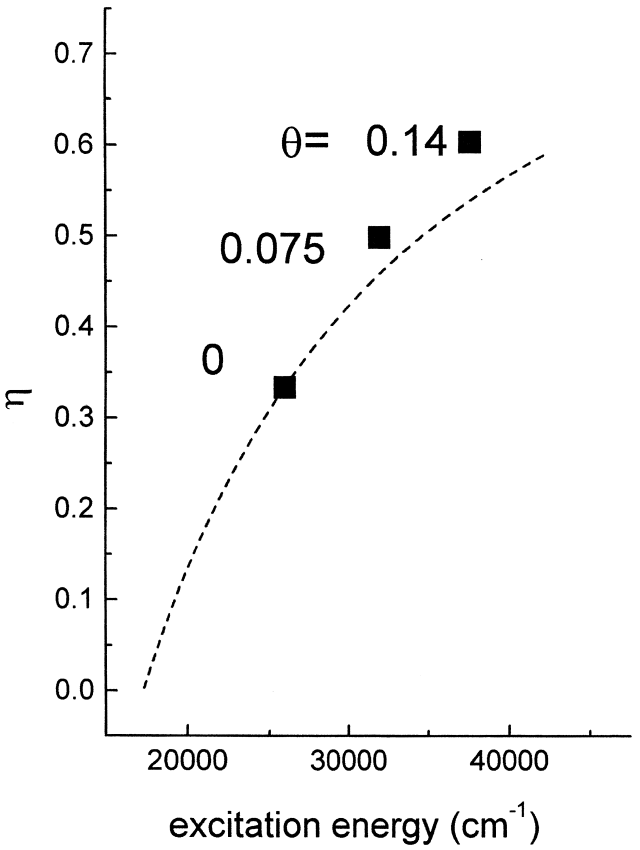

Fig. 3. The nonradiative transition efficiency calculated according to relation (6). Full squares correspond to the experimental data.

and ground electronic manifolds that take place during as well as after thermalization in the metastable state. When these processes are taken into account the heat emitted per photon is given by the following more complicated formula:

$$\eta_1(\hbar\Omega) = \frac{\hbar\Omega - \hbar\Omega_{\mathrm{lum}} + \theta(\hbar\Omega - \hbar\Omega_{\mathrm{lum}})\cdot\hbar\Omega_{\mathrm{lum}} + \vartheta\cdot\hbar\Omega_{\mathrm{lum}}}{\hbar\Omega}. \quad (8)$$

Here $\theta(\hbar\Omega - \hbar\Omega_{\mathrm{lum}})$ is the probability of the internal conversion from the excited to the ground electronic manifold that takes place before thermalization of the system in the metastable excited state (the fast processes) and ϑ is the probability of the nonradiative processes in the metastable state (the slow process). Detailed description of the kinetics of the fast and slow nonradiative processes is given in Ref. [7]. Since the probability of the fast internal conversion usually increases with energy of the excitation [7], we consider this process as responsible for steeper rise of the experimental nonradiative transitions efficiency. Assuming $\vartheta = 0$ one obtains $\theta_{\mathrm{d}_2}(32{,}000\ \mathrm{cm}^{-1}) = 0.075$ and $\theta_{\mathrm{d}_3\mathrm{d}_4}(37{,}800\ \mathrm{cm}^{-1}) = 0.14$. One has to notice that under assumption $\theta = 0$, the non-zero ϑ yields slower rise of η_1 than η.

5. Analysis of the hot luminescence

Having the configurational coordinate diagram one can consider the intensity and the kinetics of the hot luminescence, the radiative transition from the d_2 excited state to the $^2\mathrm{F}$ ground state (see Ref. [6] and Fig. 2). The hot luminescence lineshape, that is very similar to the ordinary luminescence ($\mathrm{d}_1 \rightarrow {}^2\mathrm{F}_{5/2} - {}^2\mathrm{F}_{7/2}$) lineshape suggests that the d_2 state has to be also the metastable state. It means that the excited system has enough time in the zero-phonon state of the d_2 electronic manifold to decay radiatively through $\mathrm{d}_2 \rightarrow 4\mathrm{f}({}^2\mathrm{F}_{5/2} - {}^2\mathrm{F}_{7/2})$ transition. On the other hand the intensity of the hot luminescence is about 1000 times weaker than ordinary luminescence, also the hot luminescence decay time is only in the 40 ps range [6]. Both these facts evidence that the dominating process in the d_2 state is the nonradiative internal conversion to the d_1 electronic manifold. Considering the configurational coordinate diagram presented in Fig. 2 one can see that the crossing of the d_2 and d_1 electronic manifolds appears exactly in the minimum energy of the d_2 state. It is not evident that in the system the lifetime of the zero-phonon level of the d_2 state is long enough to yield the hot luminescence of the respective lineshape. This is a reason why we consider the deexcitation processes in the d_2 and d_1 states more carefully.

The radiative deexcitation rate of the system occupying the d_2 state, P_2, is given by following relation:

$$P_2(T) = \frac{P_2^{\mathrm{rad}}}{P_2^{\mathrm{rad}} + P_{21}^{\mathrm{nrad}}(T)} \quad (9)$$

where T is temperature. P_2^{rad} is a probability of the radiative $\mathrm{d}_2 \rightarrow 4\mathrm{f}({}^2\mathrm{F}_{5/2} - {}^2\mathrm{F}_{7/2})$ transition, and $P_{21}^{\mathrm{nrad}}(T)$ is the temperature dependent probability of the nonradiative process given by

$$P_{21}^{\mathrm{nrad}}(T) = \frac{\sum_n e^{-\frac{n\hbar\omega}{kT}} W^{nm}}{\sum_n e^{-\frac{n\hbar\omega}{kT}}}. \quad (10)$$

The probability of the internal conversion between particular vibronic states is given by

$$W^{nm} = f\cdot\left|\int \chi_2^n(Q)\chi_1^m \mathrm{d}Q\right|^2 \cdot \delta(E_1^m - E_1^n). \quad (11)$$

The quantity f is called the frequency factor and describes the mixing of the electronic part of the wave functions of the system in d_1 and d_2 states [8]. Radiative transition rate P_2^{rad} can be estimated if the probability of the radiative transition from the d_1 state to the ground state, P_1^{rad}, is known. Considering that radiative transitions

between the d_2 and d_1 states and the ground state are of the same type one calculates $P_2^{rad} = P_1^{rad}(\hbar\Omega_2/\hbar\Omega_1)^3$ where $\hbar\Omega_2$ and $\hbar\Omega_1$ are energies of respective photons. Using $\hbar\Omega_2 = 25{,}730$ cm^{-1} [6], $\hbar\Omega_1 = 17{,}314$ cm^{-1} and $P_1^{rad} = 15\times10^6$ s^{-1} [2] one obtains $P_2^{rad} = 5\times10^7$ s^{-1}. The frequency factor is related to the type of interaction between initial and final electronic states, given by respective matrix elements H_{12}

$$f = \frac{2\pi}{\hbar}\frac{H_{12}^2}{\hbar\omega}. \quad (12)$$

Assuming that the mixing is caused by the spin-orbit interaction one obtains $f \approx 3\times10^{13}$ s^{-1} [9]. Finally one can calculate the dependence of the hot luminescence decay time on temperature from the relation $\tau_h(T) = 1/(P_2(T))$.

We have considered the data listed above as reliable, therefore we have performed calculations of the hot luminescence kinetics in the YAG:Ce^{3+} system using the relative electron–lattice coupling energy, $S_{21}\hbar\omega$, taken as the only free parameter of the model. The overlap integrals were calculated using the harmonic oscillator wave functions describing the vibrations in the d_1 and d_2 states. The squares of the overlap integrals between the d_2, d_1 oscillation wave functions, for different relative electron–lattice coupling strengths are presented in Fig. 4a. The respective configuration coordinate diagrams are presented in Fig. 4b. One should notice that the vibronic overlap integrals depend only on the electron lattice coupling energy and phonon energy, so the curves presented in Fig. 4a are quite universal. It is easy to find that using the radiative transitions rate and the frequency factor listed above with the strength of the electron–lattice coupling as it is presented in Fig. 2 we cannot get the effective hot luminescence even so weak as it has been measured [6]. For the electron–lattice coupling equal to 8000 cm^{-1} we have obtained the lifetime of the d_2 state approximately equal to 10^{-13} s instead of the measured hot luminescence lifetime that is about 40 ps [6]. Moreover the vibronic overlap integral is already the largest in the d_2 zero-phonon state. In such a case if the hot luminescence takes place their lifetime does not depend on temperature. To get the decrease of the hot luminescence lifetime with temperature we need significant increasing of vibronic overlap integrals in the excited phonon states with respect to the zero-phonon state. This suggests much weaker relative electron–lattice coupling between d_2 and d_1 than has been detected from consideration only of the fully symmetrical lattice mode. Actually the best fit of the calculated dependence of the hot luminescence decay time on temperature to the experiment has been obtained for the effective electron–lattice coupling $S_{12}\hbar\omega = 4500$–4750 cm^{-1} (see Fig. 5).

The inconsistency in estimations of the electron–lattice interaction energy in the excited states of the Ce^{3+} ion can be explained by the effect of the coupling of excited states to the non-symmetrical vibration modes. One considers that d_2 and d_1 states are in fact the components of the d orbital occupied by a single electron. Actually other d_1 systems (like Ti^{3+} V^{4+}) manifest usually the Jahn–Teller effect [10,11]. We expect the same in the d_1 d_2 states in the case of Ce^{3+}. Actually since d_1 and d_2 states are probably not degenerated one does not have to deal with typical Jahn–Teller effect, but still one can consider the effect as a coupling to the Jahn–Teller mode. The new mode can be described by a single effective configuration coordinate Q_{J-T} which has to be orthogonal to the coordinate Q_{A_1} describing the breathing mode [12]. Using $S_1\hbar\omega = 2225$

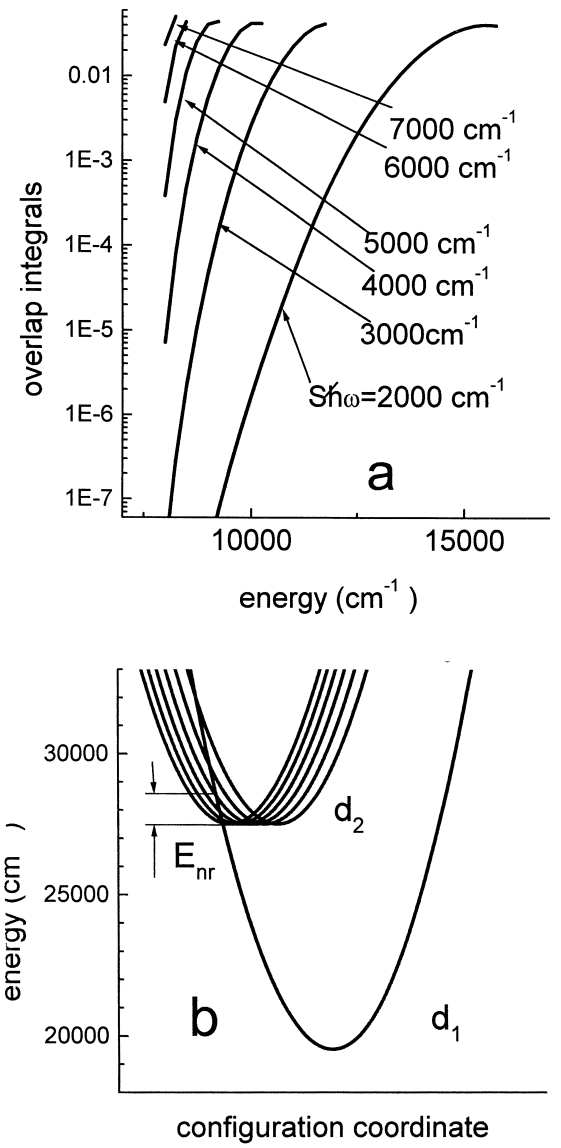

Fig. 4. (a) Squares of the vibronic overlap integrals of the d_2, d_1 system versus energy for different relative electron–lattice coupling. Energy of the minimum of the d_2 electronic manifold is 8000 cm^{-1}. For calculation of the vibronic overlap integral the effective energy of the phonon mode has been taken as $\hbar\omega = 250$ cm^{-1}. (b) Configuration coordinate diagrams corresponding to the overlaps from (a).

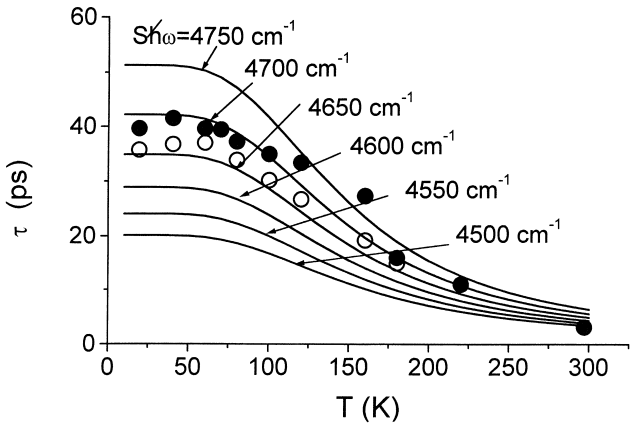

Fig. 5. Dependence of the hot luminescence decay on temperature. Solid curves represent calculated dependence (see the text), circles correspond to the experimental data taken from Ref. [6]. Open circles correspond to the hot luminescence lifetimes, full circles correspond to the ordinary luminescence risetimes.

cm^{-1}, $S_2\hbar\omega = 1785\ cm^{-1}$ and $S_{21}\hbar\omega = 4675\ cm^{-1}$ one can calculate the contribution from the Jahn–Teller coupling to the total electron–lattice coupling in particular states. Let us analyse the possible positions of the minimums energy of the ground and d_1 and d_2 excited states in the two-dimensional configurational coordinate space (see Fig. 6a). Fortunately the ground state is the f state which is not coupled to the lattice. This is a reason that the positions of the minimums energy of the d_1 and d_2 excited states can be unambiguously represented in the two-dimensional configuration space by their distances from the minimum of the ground state. Since the distance between d_1 and d_2 minimums is constants, all positions form the triangle that is fixed in the (0,0) point. The spectroscopic data will not change when the 'triangle' is rotated around the (0,0) point, although the angle of rotation changes the distribution of the electron–lattice coupling energy between the coupling to the breathing

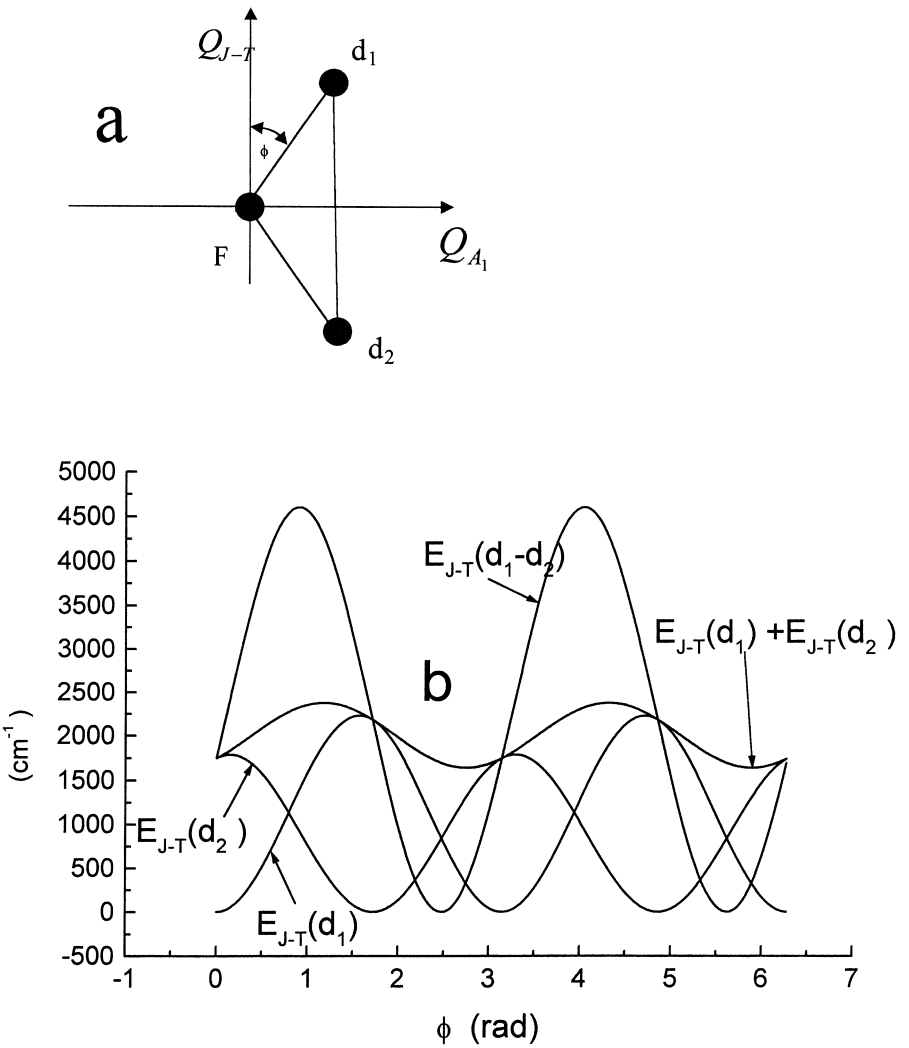

Fig. 6. (a) Positions of the minima energy of ground (F) and d_1 and d_2 electronic manifolds in the two dimensional configuration space. Each position is represented by a vector of coordinates Q_{A_1} and Q_{J-T}. (b) Jahn–Teller coupling energies as a function of positions of the minima, represented by the rotation angle, ϕ.

mode and Jahn–Teller mode in each individual excited state. One defines these energies as $E_{A_1} = Q^2_{A_1}/2$ and $E_{J-T} = Q^2_{J-T}/2$, respectively. Calculated contributions from the coupling to the Jahn–Teller mode, the energies $E_{J-T}(d_1)$, $E_{J-T}(d_2)$ and $E_{J-T}(d_1,d_2)$ are presented in Fig. 6b. Actually we do not know the contributions from the Jahn–Teller coupling to the electron–lattice interaction energy in the individual states. In Fig. 6b it is seen that these contributions can extend over the full energy range. However the quantity $E_{J-T}(d_1) + E_{J-T}(d_2)$ that is a sum of the Jahn–Teller coupling energies in the excited states is more stable. This effect can be considered as a proof of existence of the Jahn–Teller type coupling in the excited states of the Ce^{3+} ion.

6. Conclusions

We have presented the absorption, emission and photoacoustic spectra of the YAG:Ce^{3+} system. Based on these data we have obtained the energetic structure of the Ce^{3+} system in the form of the configuration coordinate diagram. Detailed analysis of the kinetics of the radiative and nonradiative processes in the excited states has shown that the single-dimensional configuration coordinate diagram cannot represent the proper structure of the excited d_1 and d_2 states. We need also to consider a coupling of the system to the Jahn–Teller type mode. Considering the absorption and photoacoustic spectra we have shown a decrease of quantum efficiency of the Ce^{3+} from 1 to 0.85 when the system is excited in the UV region by d_3 and d_4 states.

Acknowledgements

This contribution is supported in part by the Polish Committee for Scientific Research Grant 2P03 B003 13 and Gdansk University Grant 5200-5-0006-9. The authors would like to thank J. Kisielewski MSc from the Institute of Electronic Materials Technology for sample preparation.

References

[1] S.M. Kaczmarek, D.J. Sugak, A.O. Matkowskii, Z. Moroz, M. Kwaśny, A.N. Durygin, Nucl. Instrum. Methods B132 (1997) 647.
[2] J. Barzowska, A. Kubicki, M. Grinberg, S. Kaczmarek, Z. Łuczyński, A.J. Wojtowicz, Cz. Koepke, Acta Phys. Pol. A95 (1999) 396.
[3] A. Rosencwaig, A. Gersho, J. Appl. Phys. 47 (1976) 64.
[4] F. McDonald, G. Wetsel, J. Appl. Phys. 49 (1978) 2313.
[5] W.F. Krupke, M.D. Shinn, J.E. Marion, J.A. Caird, S.E. Stokowski, J. Opt. Soc. Am. B3 (1986) 557.
[6] Y. Suzuki, T. Sakuma, M. Hirai, Mater. Sci. Forum 239–241 (1997) 219.
[7] M. Grinberg, A. Mandelis, Phys. Rev. B 49 (1994) 12496.
[8] M. Grinberg, A. Mandelis, K. Fieldsted, Phys. Rev. B 48 (1993) 5935.
[9] M. Grinberg, W. Jaskólski, P.I. Macfarlane, K. Holliday, J. Phys. Cond. Matter 9 (1997) 2815.
[10] P. Albers, E. Stark, G. Huber, J. Opt. Soc. Am. B 3 (1986) 134.
[11] M. Grinberg, A. Brenier, G. Boulon, C. Pedrinini, C. Madej, A. Suchocki, J. Phys. I France 3 (1993) 1973.
[12] M. Grinberg, Cz. Koepke, J. Appl. Spectrosc. 62 (1995) 97.